Low-Momentum K^--He^4 Scattering*

P. O. Mazur, M. M. Block, J. Keren, and S. L. Meyer
Physics Department, Northwestern University, Evanston, Illinois 60201
(Received 21 August 1969)

We have measured the differential cross section for elastic scattering of K^- mesons on He^4 in the momentum intervals 100–150 MeV/c and 150–200 MeV/c, and the total inelastic cross section in the interval 150–200 MeV/c. We have calculated scattering lengths for the K^--He^4 system using the zero-effective-range approximation. The results for the scattering lengths have been compared with other experiments, including a measurement of K^--mesonic x rays in He^4. Our results are in disagreement with the latter.

I. INTRODUCTION

LOW-ENERGY scattering experiments of negative mesons on light nuclei may be used both to shed light on the meson-nucleon interaction and to relate the energy level shifts and widths in the mesonic atom[1] to the strong interactions of the meson with the nucleus.

The published x-ray experiment[2] on the K^--He mesonic atom has caused some controversy since the small level shift reported could not be related by theoretical considerations to the known $\bar{K}$*-nucleon* scattering lengths.[3] We report here a measurement of the differential cross section for elastic scattering of K^- mesons on He^4 in the momentum intervals $p_K = 100$–150 and 150–200 MeV/c and the total inelastic cross section in the interval 150–200 MeV/c. We have obtained the scattering lengths for the K^--He^4 system using the zero-effective-range approximation.

II. EXPERIMENT

We exposed the Northwestern University 20-in. helium bubble chamber to the 28° low-momentum ($\sim$750 MeV/c) separated K^- beam from the Argonne National Laboratory Zero Gradient Synchrotron which stopped in the bubble chamber after being degraded by Cu absorber. The magnetic field in the chamber was 23.7 kG. The film was scanned in three views with an over-all efficiency of 0.955 ± 0.016. Stopping K^- were uniquely identified visually by means of their distinctive ionization and curvature. Selected events and beam tracks were measured on film-plane-digitizer machines of the Franckenstein type.

Events were required to satisfy the following criteria:

(1) The scattering vertex had to be within the fiducial volume. With our choice of fiducial volume, it was possible to measure and successfully reconstruct all such events.

(2) We arbitrarily imposed a minimum c.m. system scattering-angle cut of $\cos\theta<0.9$ for the events in our final sample to avoid scanning bias for small-angle scatters. For the region $0.9>\cos\theta\geq 0.7$, a cut was imposed on the azimuthal angle to avoid a scanning bias due to dipping tracks. This restriction corresponded to a correction of approximately 26% in this $\cos\theta$ interval.

(3) The scattered K^- had to be consistent with *stopping* within the fiducial volume. The restriction to stopping K's enabled us to measure the momentum of the scattered K^- from range and permitted the imposition of a very tight constraint on our events. These were all one-constraint class events with the recoil required to be consistent.

(4) The K^- ending had to be other than a single charged prong. This completely eliminated the possibility that a stopping π^- could be misidentified as a K^-. In addition, the ending with no visible secondaries was rejected as was the ending consisting of a proton (or other baryon) plus a visible Λ^0. These restrictions eliminated (a) the possibility of K^- decays in flight contaminating our sample, (b) the possibility that $\Sigma^\pm$ production and subsequent decay could be confused with a K^- scatter, (c) the possible confusion of a K^- which scatters twice elastically, comes to rest, and emits a Λ^0 only, with the case where a K^- scatters once elastically, comes to rest and emits a proton and a Λ^0. This eliminates the necessity for the measurement of the secondaries to distinguish these two cases.

(5) Events were selected for which the potential unscattered K^- stopping vertex was within the fiducial volume.

The beam tracks used to normalize the elastic scattering cross sections were required to end within the fiducial volume and be consistent with a stopping K^-. Requirements on the beam track endings were identical with those of (4). The fractions of endings represented by the various topologies were compared for the elastic scattering events and for their associated beam tracks and were verified to be completely consistent. The procedure also tended to cancel out of the ratio of scatterings to beam track length (which determine the absolute cross sections) any potential biases in the identification of endings. The fiducial

* Supported in part by the Office of Naval Research.
[1] S. Deser, M. L. Goldberger, K. Baumann, and W. Thirring, Phys. Rev. **96**, 774 (1954).
[2] G. R. Burleson, D. Cohen, R. C. Lamb, D. N. Michael, R. A. Schluter, and T. O. White, Jr., Phys. Rev. Letters **15**, 70 (1965); D. N. Michael, Phys. Rev. **158**, 1343 (1967).
[3] F. von Hippel and J. H. Douglas, Phys. Rev. **146**, 1042 (1966); J. L. Uretsky, *ibid.* **147**, 906 (1966); J. L. Uretsky, in *High Energy Physics and Nuclear Structure*, edited by G. Alexander (North-Holland Publishing Co., Amsterdam, 1967), p. 395.

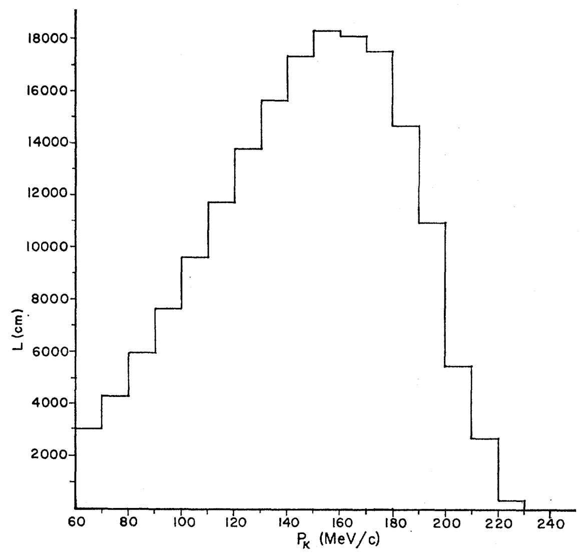

FIG. 1. Momentum distribution of the K^- beam for the K^--He^4 elastic cross-section determination.

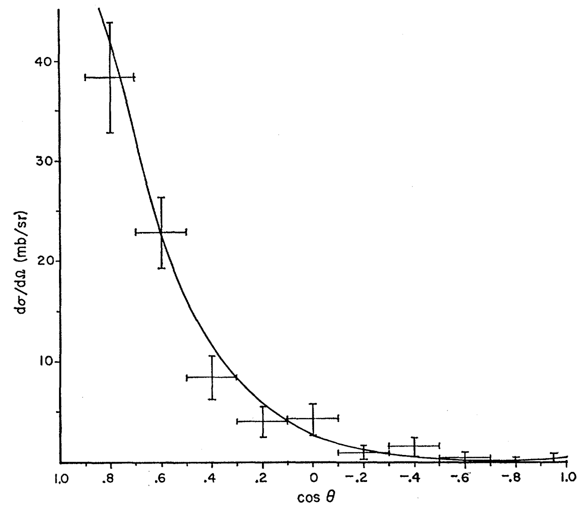

FIG. 3. Differential elastic scattering cross section in the center-of-momentum system for $150 \leq p_K < 200$ MeV/c. The curve represents Solution II.

volume restrictions permitted a systematically clean measurement of absolute cross section with small and determinate geometrical corrections.

After all the above criteria were applied there remained a sample of 322 elastic scattering events in the momentum region 100–200 MeV/c. 630 beam tracks were measured for the determination of the differential cross section; the path length distribution for this part of the experiment is shown in Fig. 1. The differential cross section measured in the momentum interval 100–150 MeV/c is plotted in Fig. 2 and that in the interval 150–200 MeV/c is shown in Fig. 3.

We have also measured the total inelastic cross section. To be accepted, tracks were required to interact within the fiducial volume and to have a potential stopping vertex within the fiducial volume. In addition, events with topological endings $\pi^- + \pi^+ + \pi^-$ and π^- only were excluded from the sample in order to eliminate contamination from K^- decay. Of necessity, we had to use the unfitted K^- momentum for the inelastic cross-section determination. The momentum at the vertex of each event was converted to a residual range giving the range histogram plotted in Fig. 4. The smooth curve is the normalized theoretical expectation for the residual range distribution of *stopping* K^- after folding in measurement and multiple-scattering errors. The

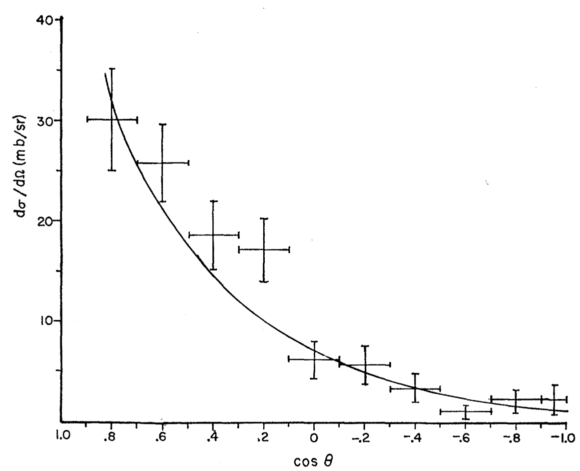

FIG. 2. Differential elastic scattering cross section in the center-of-momentum system for $100 \leq p_K < 150$ MeV/c. The curve represents Solution II.

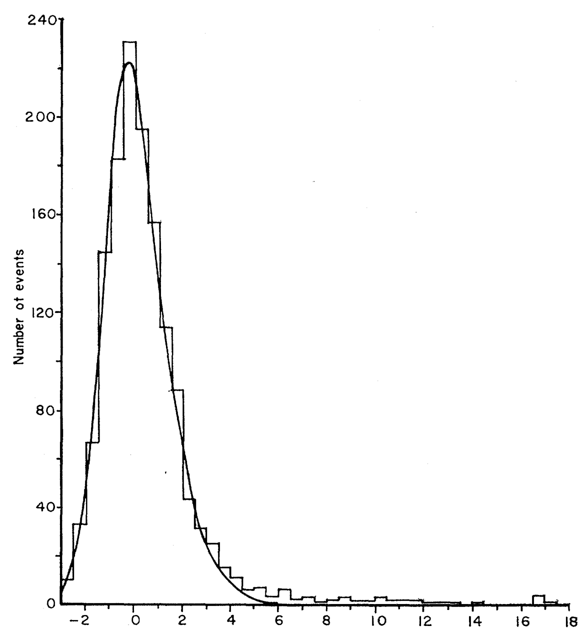

FIG. 4. Residual range distribution of elastic candidate events. The curve represents the expected distribution for stopping events.

TABLE I. Phase shifts (degrees) for the low- and high-momentum bins fitted separately.

	Solution L	Solution $H1$	Solution $H2$
$\mathrm{Re}\delta_0$	-39.2 ± 11.3	-36.3 ± 6.7	30.9 ± 9.1
$\mathrm{Im}\delta_0$	$7.0_{-7.0}^{+27.4}$	$4.4_{-4.4}^{+9.2}$	$6.8_{-6.8}^{+14.6}$
$\mathrm{Re}\delta_1$	-9.8 ± 14.7	-20.4 ± 6.5	15.1 ± 9.1
$\mathrm{Im}\delta_1$	15.8 ± 14.0	16.9 ± 11.2	19.3 ± 14.2
$\mathrm{Re}\delta_2$		-1.7 ± 3.4	-0.5 ± 3.3
$\mathrm{Im}\delta_2$		9.1 ± 4.4	7.9 ± 4.6

normalization was made to the observed number of events with residual range <3 cm. The excess of events above the theoretical curve for range >3 cm represents the number of inelastic K^- events. The cross section obtained was relatively insensitive to the lower momentum cutoff. We chose 6.2 cm as our lower cutoff, giving us 35 events in the momentum interval 150–200 MeV/c, of which we estimate 1 to be "spillover" from stopping events. This resulted in a total inelastic cross section $\sigma_{\mathrm{inel}}=250\pm44$ mb for this momentum interval.

It is obvious from an inspection of Fig. 4 that the vast majority of events in the region 1.5–6.2 cm (corresponding to the momentum interval 100–150 MeV/c) are due to stopping K^- mesons and not due to inelastic events. Thus, we are incapable of measuring the inelastic cross section in the region 100–150 MeV/c.

III. ANALYSIS

We make an expansion of the scattering amplitude $f(\theta)$ as a function of θ, the kaon scattering angle in the center-of-momentum (c.m.) system of the K^--He^4,

$$f(\theta)=\frac{1}{k}\sum(2l+1)\left(\frac{\exp(2i\alpha_l)-1}{2i}\right)P_l(\cos\theta)\,, \qquad (1)$$

where k is the c.m. momentum (units $\hbar=c=1$) and α_l is the total phenomenological phase shift which may be considered to be the sum of a Coulomb part and a phase shift due to the strong interaction in the presence of the electromagnetic field:

$$\alpha_l=\sigma_l+\delta_l\,.$$

Here, σ_l is the Coulomb phase shift and δ_l is the (Coulomb-distorted) nuclear phase shift.[4,5]

TABLE II. Scattering lengths (F) for simultaneous fit of low- and high-momentum bins.

	Solution I ($\chi^2=17.3$)	Solution II ($\chi^2=17.8$)
$\mathrm{Re}a_0$	-1.04 ± 0.21	-0.16 ± 0.94
$\mathrm{Im}a_0$	$-0.86_{-0.86}^{+0.88}$	-1.65 ± 0.21
$\mathrm{Re}a_1$	$(-0.17\pm0.35)\times10^{-3}$	$(-0.34\pm0.25)\times10^{-3}$
$\mathrm{Im}a_1$	$(-0.83\pm0.17)\times10^{-3}$	$(-0.78\pm0.16)\times10^{-3}$
$\mathrm{Re}a_2$	$(0.70\pm2.05)\times10^{-7}$	$(-2.89\pm1.92)\times10^{-7}$
$\mathrm{Im}a_2$	$(-4.55\pm1.20)\times10^{-7}$	$(-3.44\pm1.05)\times10^{-7}$

[4] M. M. Block, Phys. Letters **25B**, 604 (1967).

[5] D. Koetke, Ph.D. thesis, Northwestern University, 1968 (unpublished).

We may then write

$$f(\theta)=f_c(\theta)+f_N(\theta)\,,$$

where

$$f_c(\theta)=\frac{1}{k}\sum(2l+1)P_l(\cos\theta)\left(\frac{\exp(2i\sigma_l)-1}{2i}\right)$$
$$=\frac{\eta}{2k\sin^2(\frac{1}{2}\theta)}\exp[2i(\sigma_0+\eta\ln\sin\tfrac{1}{2}\theta)] \qquad (2)$$

and

$$f_N(\theta)=\frac{1}{k}\sum(2l+1)P_l(\cos\theta)$$
$$\times\exp(2i\sigma_l)\left(\frac{\exp(2i\delta_l)-1}{2i}\right). \qquad (3)$$

Here

$$\eta=Z\alpha/\beta_{\mathrm{rel}}$$

(where $\beta_{\mathrm{rel}}=$ relative K-He^4 velocity in the c.m. system and $\alpha=$ fine-structure constant),

$$\sigma_l=\arg\Gamma(l+1-i\eta)\,,$$

and, for this experiment, $Z=2$, $\eta\sim0.06$, i.e., $\eta\ll1$. The differential cross section is

$$d\sigma/d\Omega=|f_c(\theta)+f_N(\theta)|^2\,. \qquad (4)$$

We may express $f_N(\theta)$ in terms of the complex partial-wave scattering amplitudes

$$T_l=(e^{2i\delta_l}-1)/2i\,. \qquad (5)$$

We then write the total inelastic cross section, in the limit of $\eta\ll1$, as

$$\sigma_{\mathrm{inel}}=(4\pi/k^2)\sum(2l+1)(\mathrm{Im}T_l-|T_l|^2)\,. \qquad (6)$$

We have fitted our data with this partial-wave expansion. The low-momentum data ($100\leq p_K<150$ MeV/c, $\bar{k}=0.5700$ F^{-1}, where p_K is the lab momentum and $\bar{k}$ is the average c.m. momentum) required s and p waves only. Only one good fit (L) was obtained for the low-energy data in the sense of having a χ^2 minimum. For solution L, $\chi^2=4.0$ for six degrees of freedom. One cannot, however, exclude other solutions on the basis of the magnitude of χ^2.

The high-momentum data ($150\leq p_K<200$ MeV/c, $\bar{k}=0.7693$ F^{-1}) were fitted with the additional information of the total inelastic cross section. Two solutions ($H1$ and $H2$) with good χ^2 probability and well-defined χ^2 minima were obtained, although s, p, and d waves were required. Solutions with s and p waves alone were excluded on the basis of χ^2. Solutions $H1$ and $H2$ have χ^2 values of 3.5 and 3.7, respectively, for five degrees of freedom. The phase shifts for solutions L, $H1$, and $H2$ are given in Table I.

In order to fit with a minimum number of parameters and tie together the corresponding phase shifts in the two momentum intervals 100–150 MeV/c and 150–200 MeV/c, we employ the zero-effective-range hypothesis

TABLE III. Energy level shift and widths for the K^--He^4 atomic system.

	Solution I	Solution II	K^--He^4 x-ray experiment	K^--He^4 scattering experiment (Ref. 8)
ΔE_{1s} (keV)	6.27 ± 1.28	0.94 ± 5.67	<0.4	-1 ± 8
Γ_{1s} (sec^{-1})	$(1.57_{-1.57}^{+1.61})\times 10^{19}$	$(3.02 \pm 0.38)\times 10^{19}$	$<2\times 10^{18}$	$(1.4\pm 1)\times 10^{19}$
Γ_{2p} (sec^{-1})	$(1.43 \pm 0.29)\times 10^{15}$	$(1.34 \pm 0.27)\times 10^{15}$	$(1.0_{-0.6}^{+1.5})\times 10^{13}$	$(1.1\pm 0.4)\times 10^{15}$
Γ_{3d} (sec^{-1})	$(3.80 \pm 1.00)\times 10^{10}$	$(2.87 \pm 0.88)\times 10^{10}$		
Fraction of K^- in $2p$ state which are absorbed	0.994 ± 0.001	0.994 ± 0.001	$0.54_{-0.22}^{+0.21}$	>0.98
Fraction of K^- in $3d$ state which are absorbed	0.041 ± 0.010	0.031 ± 0.009		

and analyze our data in terms of s-, p-, and d-wave scattering lengths, which are necessarily complex. Pure nuclear scattering lengths A_l are defined by

$$k^{2l+1}\cot\Delta_l = -1/A_l B^{2l}, \tag{7}$$

where B = Bohr atomic radius for the K^--He^4 system = 31 F, and Δ_l is the pure nuclear phase shift. Following the treatment of Trueman[6] which takes into account the Coulomb distortion of the nuclear phases for s and p waves, we replace (7) by the expressions[6]

$$\frac{1}{B}\left(\frac{C_0^2(\eta)\cot\delta_0}{\eta} - 2h(\eta)\right) = -\frac{1}{a_0}, \tag{8}$$

$$\frac{1}{B}\left[\frac{C_1^2(\eta)\cot\delta_1}{\eta^3} - 2h(\eta)\left(\frac{\eta^2+1}{\eta^2}\right)\right] = -\frac{1}{a_1}, \tag{9}$$

where

$$C_l(\eta) = |\Gamma(l+1+i\eta)|\, e^{\pi\eta/2}$$

and

$$h(\eta) = \eta^2 \sum_{m=1} \frac{1}{m(m^2+\eta^2)} - \ln\eta - 0.577\,,$$

and use the approximation for the d waves that $k^5\cot\delta_2 = -1/a_2B^4$.

We then fit our data with a_0, a_1, and a_2, as defined above. Solutions I and II, shown in Table II, have χ^2 values of 17.3 and 17.8, respectively, where 15 is expected. The satisfactory χ^2 obtained implies that our data are consistent with the zero-effective-range hypothesis. Solution II is plotted in Figs. 2 and 3. Solution I is not visibly different from Solution II. Solution I yields a fitted inelastic cross section of 263 mb, whereas Solution II yields 249 mb. In each case, p-wave capture predominates in our momentum region. The contributions of s, p, and d waves to the inelastic cross section for Solution II are shown in Fig. 5.

We may relate these scattering lengths to the energy levels of the K^--He^4 mesonic atom and obtain the energy level shifts $\Delta E_{n,l}$ due to strong interactions and the (strong-interaction) capture rates from the ns and np states. The relation is, to first order in A/B,

$$\frac{\Delta E_n}{E_n} = \frac{-4A_0}{nB} \quad \text{for } s \text{ states},$$
$$\frac{\Delta E_n}{E_n} = -\left(1-\frac{1}{n^2}\right)\frac{4A_1}{nB} \quad \text{for } p \text{ states}, \tag{10}$$

where E_n = energy of state in question $= 1/n^2(2\mu B^2)$, B = Bohr radius, A = (complex) scattering length, $\mu = K^-$-He^4 reduced mass.

As shown in the Appendix, for small A_l/B, we can write, in general,

$$\frac{\Delta E_{n,l}}{E_{n,l}} = -\frac{4}{n}\frac{A_l}{B}\left(\frac{1}{l!}\right)^2 \prod_{i=0}^{l}\left(1-\frac{i^2}{n^2}\right). \tag{11}$$

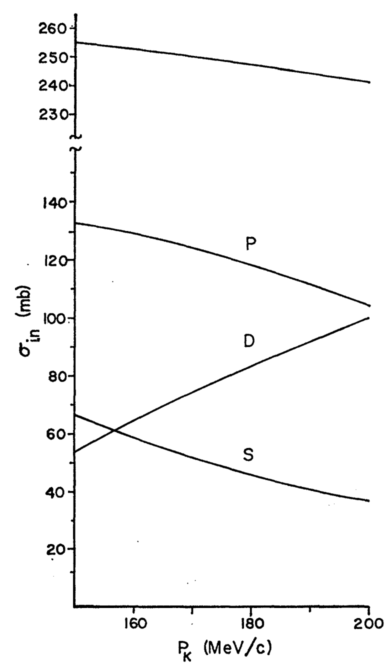

FIG. 5. Contributions to the inelastic cross section due to s, p, and d waves for Solution II.

[6] T. L. Trueman, Nucl. Phys. **26**, 57 (1961). Note that this reference paper contains a typographical error for the relation between the s-wave phase shift and the s-wave scattering length. The correct defining equation is $(1/B\eta)C_0^2(\eta)\cot\delta_0 - 2h(\eta)/B = -1/a_0 + \frac{1}{2}r_0k^2$, where the various quantities are as defined in Trueman's paper.

TABLE IV. Phase shifts (in deg) for simultaneous fit of low- and high-momentum bins.

	100–150 MeV/c		110–160 MeV/c	150–200 MeV/c	
	Solution I	Solution II	Ref. 8	Solution I	Solution II
$\mathrm{Re}\delta_0$	37.0 ± 8.3	50.8 ± 22.3	undetermined	45.0 ± 11.0	66.1 ± 27.3
$\mathrm{Im}\delta_0$	17.0 ± 17.0	50.8 ± 42.5	$12<\mathrm{Im}\delta_0$	17.2 ± 15.8	41.1 ± 19.0
$\mathrm{Re}\delta_1$	2.5 ± 4.2	4.5 ± 2.8	$-12<\mathrm{Re}\delta_1<14$	7.8 ± 10.0	12.3 ± 6.0
$\mathrm{Im}\delta_1$	10.0 ± 2.4	9.2 ± 2.1	$14<\mathrm{Im}\delta_1<27$	23.9 ± 7.8	20.9 ± 6.1
$\mathrm{Re}\delta_2$	-0.2 ± 0.6	0.9 ± 0.6		-1.0 ± 3.0	4.1 ± 2.7
$\mathrm{Im}\delta_2$	1.4 ± 0.4	1.1 ± 0.3		6.5 ± 1.7	4.9 ± 1.5

We neglect the small (order of η) electromagnetic difference between A_l and a_l.[7] For the above, n is the principal quantum number of the level and l is the angular momentum quantum number. Since the A_l are complex, the real portion of $\Delta E_{n,l}$ represents the energy shift of the level due to the nuclear forces, and the imaginary part corresponds to the level width $\frac{1}{2}\Gamma$, where Γ is the nuclear absorption rate.

For our experiment, we get the results summarized in Table III.

IV. DISCUSSION

We have summarized the experimental results of another measurement[8] of K^--He^4 scattering in Tables III and IV. Apart from improvements in the procedures of our experiment, as detailed in Sec. II, our experiment differs from that of Ref. 8 in that we have approximately three times as many elastic scattering events, and we are therefore able to separate our data into two momentum regions. Because of our increased sensitivity in the higher-momentum bin, we were able to demonstrate the need for d waves in the fit. The other experiment needed only s and p waves, even though the inelastic cross section determined in that experiment is 350 ± 70 mb, which is very close to the s- and p-wave unitarity limit of 346 mb for their average momentum. Using the zero-effective-range hypothesis we are also able to determine both the sign and magnitude of the real part of the phase shifts, as shown in Table IV, whereas the other experiment was unable to measure $\mathrm{Re}\delta_0$ and only obtained an upper limit to the magnitude of $\mathrm{Re}\delta_1$.

If we compare our phase shifts in the momentum interval 100–150 MeV/c with the phase shifts of Ref. 8, which refer to the nearby interval 110–160 MeV/c, we note crude agreement between the experiments for the imaginary parts of δ_0 and δ_1.

In Sec. III of this paper we presented a calculation of the complex energy level shifts (i.e., energy shift and capture rate) of the Coulomb bound states of the K^--He^4 mesonic atom, using as input the measured complex scattering lengths. These results are tabulated in Table III, along with the results of the other K^--He scattering experiment.[8,9] For comparison with the x-ray experiment,[2] we also present in Table III our values[10] for the fraction of K^- in $2p$ and in $3d$ states which are absorbed, as well as the x-ray results. Our results are not consistent with those of the published x-ray experiment. Of the K^- mesons which reach the $2p$ level, our result indicates that approximately 99% are captured, and therefore the K_α line should not have been observed in the intensity claimed in the x-ray experiment.

As mentioned in Sec. III, p-state capture dominates the inelastic interactions in flight in our momentum region. Assuming the atomic cascade proceeds via circular orbits,[11] we also deduce that most of the kaons are captured at rest from a p state. A comparison of the absorption interactions in flight and of the capture reactions at rest should yield the same branching fractions if the angular momentum state is the same for at-rest and in-flight events. A summary of our results for the (inelastic) interactions of K^- on He^4 appears in Table V for K^- at rest and in flight (150–200 MeV/c). No inelastic events in which a kaon was emitted were observed. Table V includes events in which the Λ^0 decayed neutrally as well as into the charged mode. The salient feature of Table V is that, within statistics, the branching fractions for K^- in flight are consistent with those for K^- at rest. The assumed p-wave nature of the K^--He^4 capture from rest and the observed

[7] It has been shown (e.g., in Ref. 5) that the Coulomb-distorted nuclear phase shift may, to first order, be equated to the sum of the pure nuclear phase shift Δ_l and a term linear in the Coulomb strength parameter ξ, $\delta_l=\Delta_l-\xi x_l$, where $\xi x_l=-k\int v(r)[R_l^2(r)-j_l^2(kr)]r^2dr$, as defined in Ref. 5. We have calculated the ξx_l relevant to our experiment by the iterative procedure of Koetke (see Ref. 5) and find them to be small in comparison with the nuclear portion. For the d waves, we shall disregard the difference between the Coulomb-distorted nuclear phase shift and the pure nuclear phase shift, as well as the difference between the distorted scattering length and the pure nuclear scattering length.

[8] J. J. Boyd, R. A. Burnstein, J. G. McComas, V. R. Veirs, and G. Rosenblatt, Phys. Rev. Letters 19, 1405 (1967).

[9] It should be emphasized that all of the complex level shifts deduced from these K^--He^4 scattering experiments depend on the hypothesis of zero effective range.

[10] J. B. Kopelman, Ph.D. thesis, Northwestern University, 1965 (unpublished). We have used Kopelman's values for the radiative transition rates of K^--He^4 mesonic atoms in calculating the fraction absorbed relative to those which make the radiative transition $n, l\rightarrow n-1, l-1$.

[11] Kopelman's measurement of the cascade time of kaons in liquid helium is consistent with cascade in circular orbits via radiative and Auger transitions.

dominance of p-wave absorption in flight, for our momentum region, are thus consistent.

We may obtain from Table V the fraction of two- (or more-) nucleon absorption of K^- in He^4. We assume that absorption from a single nucleon operates via the reaction $\bar{K}+N \rightarrow Y+\pi$ and that two-nucleon capture goes via $\bar{K}+2N \rightarrow Y+N$. Thus, the number of events with no pions over the total number of events yields the required fraction of two nucleon captures if we assume that there is no pion reabsorption in the He^4 nucleus.

We determine the number of neutral pions by use of charge independence: $n(\pi^0)=\frac{1}{2}[n(\pi^+)+n(\pi^-)]$. For the at-rest events, this predicts that $\frac{1}{2}(647)=324$ of the "events without $\pi^\pm$" are really neutral pion events. As a check on this, we note that our sample contained four events with a Dalitz pair. Further, none of these contained $\pi^\pm$. This is completely consistent with the $\sim 1/80$ branching fraction for π^0 decay to a Dalitz pair.

The number of pionic events for K^- at rest is, therefore, $n(\pi^+)+n(\pi^-)+n(\pi^0)=971$, and the number of nonpionic events$=788-324=464$. The fraction of two-nucleon captures from rest is therefore 0.32 ± 0.02. For the in-flight data, the fraction is 0.27 ± 0.13.[12] Again, the results for at-rest and in-flight K^- are consistent within the (limited) statistics.

Block and Koetke[13] have published a single-scattering impulse model theory of π-He^4 scattering and, although this impulse model is not expected to be exact for $\bar{K}$-He^4 scattering, we can use the spirit of this model to attempt to relate the $\bar{K}$-nucleon scattering data to this experiment.

Kim[14] and Humphrey and Ross[15] are able to fit the low-energy $\bar{K}$-nucleon scattering data with s waves only, whereas our experiment required s, p, and d waves. Block and Koetke have found that the invariant cross section $d\sigma/dq^2$ for $\bar{K}$-He^4 scattering, where q^2 is the momentum transfer squared, is related to the spin-averaged isospin-averaged $\bar{K}$-nucleon cross section by the form factor squared, $e^{-q^2R^2/3}$, where R is the rms radius of He^4. The squared form factor may be expanded in a power series to exhibit $\cos\theta$ dependence:

$$e^{-q^2R^2/3}=e^{-2k^2R^2/3}[1+\tfrac{2}{3}k^2R^2\cos\theta+\tfrac{1}{2}(\tfrac{2}{3}k^2R^2)\cos^2\theta+\cdots].$$

Hence, higher angular momentum waves can be induced

[12] We note that the two-nucleon capture ratio of 0.32 ± 0.02 is significantly greater than the value 0.17 ± 0.04, reported by the Helium Bubble Chamber Collaboration Group [in *Proceedings of the Tenth Annual International Rochester Conference on High-Energy Physics, 1960*, edited by E. C. G. Sudarshan, J. H. Tinlot, and A. C. Melissinos (Interscience Publishers, Inc., New York, 1960), pp. 426–431]. The raw data from both experiments are in agreement, but no correction was made in the older experiment for "zero-length" Λ^0's. After application of this correction, the two-nucleon capture ratio agrees with the present value of 0.32. Thus we conclude that the two-nucleon capture process represents a very important channel in the absorption of K^- on He^4.

[13] M. M. Block and D. Koetke, Nucl. Phys. **B5**, 451 (1968).

[14] J. K. Kim, Phys. Rev. Letters **14**, 29 (1965).

[15] W. E. Humphrey and R. R. Ross, Phys. Rev. **127**, 1305 (1962).

TABLE V. Topologies of K^- absorption events in flight and at rest.

Type	Events with π^-	Events with π^+	Events without $\pi^\pm$
K^- at rest			
Λ^0 or Σ^0	356 (24.8%)	59 (4.1%)	687 (47.9%)
Σ^+	136 (9.5)	0 (0.0)	26 (1.8)
Σ^-	0 (0.0)	93 (6.5)	75 (5.2)
hypernuclei	3 (0.2)	0 (0.0)	0 (0.0)
total	495 (34.5)	152 (10.6)	788 (54.9)
K^- in flight			
Λ^0 or Σ^0	10 (28.6%)	1 (2.9%)	17 (48.6%)
Σ^+	3 (8.6)	0 (0.0)	0 (0.0)
Σ^-	0 (0.0)	3 (8.6)	1 (2.9)
hypernuclei	0 (0.0)	0 (0.0)	0 (0.0)
total	13 (37.2)	4 (11.4)	18 (51.5)

from the s-wave $\bar{K}$-nucleon cross section by the form factor. All angular momentum waves induced in this way will have the same sign. For this reason we tend to favor our Solution II over Solution I, since the latter has negative real parts for the s- and p-wave scattering lengths and positive for the real part of the d-wave scattering length, while the former has all real parts of the scattering lengths negative.

The matrix element for K^--He^4 elastic scattering is $\frac{3}{4}f_1+\frac{1}{4}f_0$, where f_1 and f_0 are non-spin-flip amplitudes for the isospin-one and isospin-zero $\bar{K}$-nucleon states, respectively. Using this impulse-model interpretation to compare the signs of our scattering lengths with the $\bar{K}$-nucleon scattering experiments, we find agreement in sign with the results of Humphrey and Ross and disagreement with those of Ref. 14.

ACKNOWLEDGMENTS

We wish to thank all of the ZGS personnel who made this exposure possible, in particular, Dr. R. D. Klem for his operation of the beam. The work of Dr. W. M. Bugg, Dr. H. O. Cohn, and Dr. G. T. Condo in tuning the beam is gratefully acknowledged. It is a pleasure to thank Dr. P. K. Malhotra, Dr. I. Spirn, Dr. H. Winzeler, and especially Dr. R. J. Walker for their work on the operation of the bubble chamber.

APPENDIX

Using first-order perturbation theory, and treating the nuclear potential U as a perturbation on bound-state hydrogenic K^--He^4 wave functions, the energy shift $\Delta E_{n,l}$ is given by

$$\Delta E_{n,l}=\int \psi_{nlm}{}^*U\psi_{nlm}d\tau\,, \tag{A1}$$

where the hydrogenlike wave function

$$\psi_{nlm}=R_{nl}(r)\Theta_{lm}\Phi_m. \tag{A2}$$

This is so normalized that

$$\int R_{nl}^2(r)r^2dr=\int |\Theta_{lm}\Phi_m|^2 d\Omega=1 \tag{A3}$$

and

$$R_{nl}(r)=-\left[\left(\frac{2}{nB}\right)^3\frac{(n-l-1)!}{2n\{(n+l)!\}^3}\right]^{1/2} \times e^{-\rho/2}\rho^l L_{n+l}{}^{2l+1}(\rho), \tag{A4}$$

where

$$\rho=2r/nB$$

and B is the Bohr radius ($B=1/Z\mu\alpha$). The associated Laguerre polynomial is given by

$$L_{n+l}{}^{2l+1}(\rho)=\sum_{k=0}^{n-l-1}(-1)^{k+1} \times\frac{[(n+l)!]^2\rho^k}{(n-l-1-k)!(2l+1+k)!k!}. \tag{A5}$$

Since the range of the nuclear potential is very much less than B, (A1), using (A2) and (A3), can be replaced by

$$\Delta E_{n,l}=\frac{1}{(l!)^2}\left|\frac{d^lR_{nl}(0)}{dr^l}\right|^2\int_0^\infty Ur^{2l+2}\,dr. \tag{A6}$$

The scattering length A_l, defined in (7), can be calculated using the Born approximation. We can rewrite (7) as

$$A_l=\lim_{k\to 0}\frac{-\Delta_l}{k^{2l+1}B^{2l}} =-\lim_{k\to 0}\left(\frac{-2\mu k}{k^{2l+1}B^{2l}}\right)\int_0^\infty Uj_l^2(kr)r^2\,dr, \tag{A7}$$

where $j_l(kr)$ is the spherical Bessel function. Thus, for small kr,

$$A_l=\frac{+2\mu}{B^{2l}[(2l+1)!!]^2}\int_0^\infty Ur^{2l+2}\,dr. \tag{A8}$$

Equating the integrals in (A8) and (A6), and using

$$E_{n,l}=-1/n^2(2\mu B^2),$$

we see that

$$\frac{\Delta E_{n,l}}{E_{n,l}}=\frac{-n^2B^{2l+2}}{(l!)^2}[(2l+1)!!]^2A_l\left|\frac{d^lR_{nl}(0)}{dr^l}\right|^2. \tag{A9}$$

Explicitly evaluating the derivatives of the radial wave function (A4), we finally obtain, after some manipulation, the result

$$\frac{\Delta E_{n,l}}{E_{n,l}}=\frac{-4}{n}\frac{A_l}{B}\left(\frac{1}{l!}\right)^2\prod_{i=0}^{l}\left(1-\frac{i^2}{n^2}\right). \tag{A10}$$

This result has been independently derived by Seki.[16]

The real part of $\Delta E_{n,l}$ represents the energy shift of the Coulomb bound state with energy $E_{n,l}$. Since $E_{n,l}$ is defined to be negative, a negative value for $\Delta E_{n,l}$ represents a more tightly bound system. The imaginary part of $\Delta E_{n,l}$ is one-half the full width of the level, and thus is also one-half the nuclear capture rate.

[16] R. Seki, Bull. Am. Phys. Soc. 14, 544 (1969).